Engineering Notes

Spacecraft Deorbit Point Targeting Using Aerodynamic Drag

Sanny R. Omar,* Riccardo Bevilacqua,†
and David Guglielmo‡
*University of Florida, ADAMUS Laboratory, Gainesville,
Florida 32611*
Laurence Fineberg§ and Justin Treptow¶
NASA Kennedy Space Center, Titusville, Florida 32899
and
Scott Clark** and Yusef Johnson††
*a.i. solutions Incorporated, NASA Kennedy Space Center,
Titusville, Florida 32899*

Nomenclature

a	=	semimajor axis, km
e	=	eccentricity
h	=	angular momentum, km^2/s
i	=	orbit inclination, rad
m	=	satellite mass, kg
r	=	orbit radius, km
t_{deorbit}	=	time at which the satellite deorbits, s
t_{swap}	=	time at which the ballistic coefficient is changed from C_{b1} to C_{b2}, s
t_{term}	=	time at which the satellite enters the terminal phase of its trajectory, s
u	=	argument of latitude, rad
v	=	orbital velocity, km/s
θ	=	true anomaly, rad
μ	=	Earth's gravitational parameter, km^3/s^2
Ω	=	right ascension of the ascending node, rad
ω	=	argument of the periapsis, rad
ω_a	=	average orbital angular velocity, rad/s

*Ph.D. Candidate, Department of Mechanical and Aerospace Engineering, 939 Sweetwater Dr., MAE-A Room 211. Student Member AIAA.

†Associate Professor, Department of Mechanical and Aerospace Engineering, 939 Sweetwater Dr., MAE-A Room 308. Senior Member AIAA.

‡Postdoctoral Research Assistant, Department of Mechanical and Aerospace Engineering, 939 Sweetwater Dr. Student Member AIAA.

§Systems Integration Engineer, Launch Services Program.

¶Flight Design Engineer, Launch Services Program.

**Project Manager.

††Flight Design Engineer.

I. Introduction

SAFE deorbiting of spacecraft parts surviving atmospheric reentry is a key focus of space programs [1,2]. When propulsion systems are not an option (due to cost or volume constraints), modulation of the aerodynamics may be a feasible way to perform reentry control. Although extensive work exists on density modeling and spacecraft drag estimation [3,4], and there is a body of research on relative spacecraft maneuvering using differential drag [5–7], only two papers can be found on a controlled deorbit algorithm utilizing solely aerodynamic drag [8,9].

The first one [8] uses NASA's Program to Optimize Simulated Trajectories II trajectory-optimization tool to calculate the ballistic-coefficient profile necessary for the spacecraft to land or break up in a desired location. The optimizer is not tuned to the specific problem, and has no guarantee of performance or convergence, making this technique unsuitable for onboard guidance generation. The second algorithm [9] uses an analytical solution to estimate the ballistic-coefficient profile needed for the spacecraft to deorbit in a desired location. This analytical solution, however, requires an exponential atmospheric-density model and the assumption of a circular orbit around a spherical Earth. These assumptions are limiting, as density can vary by over an order of magnitude at a given orbital altitude, and the orbit does not remain circular due to gravitational and aerodynamic perturbations, especially near the end of the orbit life. Additionally, the proposed analytical solution requires the evaluation of the function

$$f_t(a) = \frac{\sqrt{\pi H}\,\mathrm{erfi}(\sqrt{a/H})}{-2C_b\sqrt{\mu}\rho_0 e^{a_0/H}} \qquad (1)$$

at the initial and final spacecraft semimajor axes. In Eq. (1), H is the scale height, ρ_0 and a_0 are the reference density and semimajor axis, erfi is the imaginary error function, and C_b is defined as in [10]. At a values near the deorbit point, where H is small (below 120 km altitude), calculating $\mathrm{erfi}(\sqrt{a/H})$ leads to an overflow in MATLAB, rendering the analytical solution unusable. As such, the authors of [9] recognize that, if an accurate guidance is desired, this analytical solution is useful only as a first guess in a numerical-optimization tool, such as the one used in [8].

This paper proposes a novel algorithm that calculates the drag profile necessary for a spacecraft to deorbit in a desired location. Similar to [9], a trajectory is considered, in which the spacecraft maintains some ballistic coefficient C_{b1} until time t_{swap}, C_{b2} until time t_{term} (which occurs at some predetermined semimajor axis), and C_{b_term} until the deorbit point (around 70 km altitude). A numerical-optimization method is proposed that varies the control parameters C_{b1}, C_{b2}, and t_{swap} to minimize the function $f(C_{b1}, C_{b2}, t_{\mathrm{swap}})$, giving the error between the desired and actual deorbit points after the trajectory is numerically propagated with the chosen control parameters. This optimization procedure is fundamentally different from the state of the art and offers unique benefits. At each optimization step, an analytical solution based on a simplified orbital model is used to estimate the set of control parameters needed for optimal targeting. The procedure continues as shown in Fig. 1 until a desired error tolerance is met, or a maximum number of iterations are reached. This algorithm is analogous to the Newton–Raphson root-finding method, in which an analytically solvable approximation of a complex function is constructed at each time step to determine the next point at which the complex function should be evaluated.

The use of this analytical solution yields superior performance compared to traditional optimization methods, such as the conjugate gradient and secant methods, because it is based on orbital mechanics principles and much more closely resembles the true function than
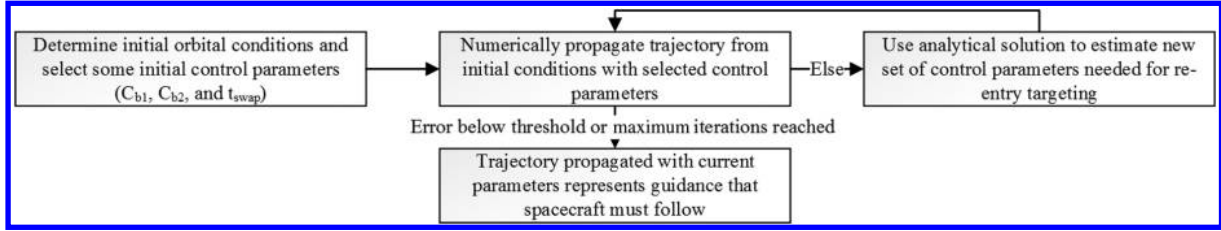
Fig. 1   Targeting-algorithm schematic.

the linear approximations used by the other methods. As such, the algorithm in this paper facilitates the rapid and reliable computation of accurate guidance trajectories. The guarantees of performance and convergence provided by the analytical solution make this algorithm potentially suitable for autonomous, onboard guidance computation.

II.   Analytical Mapping from Initial State to Impact Location

A.   Analyzing the Effects of Drag on an Orbit

Assuming circular orbit and density as function of the semimajor axis, the following relationship holds:

$$\Delta t_2 = \frac{C_{b1} \Delta t_1}{C_{b2}} \tag{2}$$

in which the Δt_1 represents the time required to decay the semimajor axis a set amount (from a_0 to a_f) with corresponding C_{b1} (see eq. 9–24 in [11]), and Δt_2 is the time required to achieve this same change in a with some different C_{b2}. Similarly, the changes in true anomaly that occur in each case are related by

$$\Delta \theta_2 = \frac{\Delta \theta_1 C_{b1}}{C_{b2}} \tag{3}$$

Dividing Eq. (3) by Eq. (2) demonstrates that the average orbital angular velocity ω_a as a spacecraft falls from a_0 to a_f is a constant independent of ballistic coefficient. Given a numerically propagated trajectory, $\dot{\Omega}_{avg}$ can also be calculated by dividing the total change in right ascension by the orbit lifetime. Over a given time interval, the change in right ascension can be approximated by

$$\Delta \Omega = \dot{\Omega}_{avg} \Delta t \tag{4}$$

B.   Analytically Calculating Reentry Location Based on Applied Controls

The targeting algorithm requires the ability to calculate where a satellite will deorbit given a set of initial conditions and applied controls (C_{b1}, C_{b2}, and t_{swap}). This can be performed by first propagating an initial trajectory and analyzing perturbations from this initial trajectory. Consider Fig. 2, in which the solid line represents a numerically propagated trajectory, in which the spacecraft maintains some ballistic coefficient C_{b1} until time t_{swap}, C_{b2} until time t_{term}, and C_{b_term} until the deorbit point. Everything about this trajectory is known, including the time, change in true anomaly, and change in right ascension between any two points. The dashed line represents a new trajectory starting from the same initial conditions, but with a different set of control parameters (C_{b1}, C_{b2}, and t_{swap}) that we would like to analyze without propagating. This new trajectory can be broken into four phases (denoted by the vertical lines in Fig. 2), in which each phase is represented by an initial and final semimajor axes, and the C_b remains constant for both the new and initial trajectories throughout the phase.

The Δt, $\Delta \Omega$, and $\Delta \theta$ during each phase of the new trajectory can be calculated using Eqs. (2–4); the known Δt, $\Delta \Omega$, $\Delta \theta$, and C_b of the initial trajectory during that phase; and the new trajectory C_b during the phase. Summing the parameter changes during each phase and assuming that the new and initial trajectories have the same initial
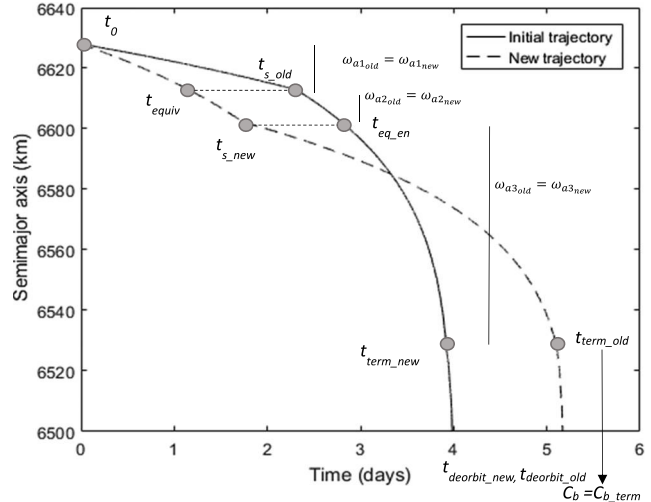

Fig. 2   Semimajor axis over time for old and new trajectories.

conditions and maintain the same inclination and eccentricity provide the time and orbital-element values of the new trajectory at the deorbit point. Note that the terminal phase (time t_{term}) occurs when the satellite reaches a given semimajor axis, and both the new and initial trajectories maintain the same C_{b_term} during this phase, and hence experience the same changes in time and orbital elements.

III.   Latitude- and Longitude-Targeting Algorithm

Using the analytical relationship between the control parameters and the deorbit location developed in Sec. II, the tasks of latitude and longitude targeting can be decoupled, making it possible to analytically calculate the control parameters needed for reentry-point targeting.

To begin, the set of t_{swap} values that yield perfect latitude targeting is calculated semi-analytically. To do this, the required argument of latitude u at deorbit must be determined. The z component of the Earth-centered inertial (ECI) position vector at the target latitude can be expressed in terms of the target latitude (lat) and the magnitude of the spacecraft position vector at the target latitude [12]:

$$R_z = r \sin(\text{lat}) = \frac{h^2}{\mu(1 + e \cos \theta)} \sin(\text{lat}) \tag{5}$$

The z component of the ECI position vector is also equal to the bottom row of the perifocal to the ECI frame direction cosine matrix given by eq. 4.49 in [12] multiplied by the perifocal position vector.

$$
\begin{aligned}
R_z &= \frac{h^2}{\mu(1 + e \cos \theta)} \sin(\text{lat}) \\
&= \frac{h^2}{\mu(1 + e \cos \theta)} [\sin(\omega) \sin(i) \quad \cos(\omega) \sin(i) \quad \cos(i)] \begin{bmatrix} \cos \theta \\ \sin \theta \\ 0 \end{bmatrix}
\end{aligned} \tag{6}
$$

Assuming that θ is the only variable changing and must be between 0 and 2π, the bisection root-finding method can be used to rapidly
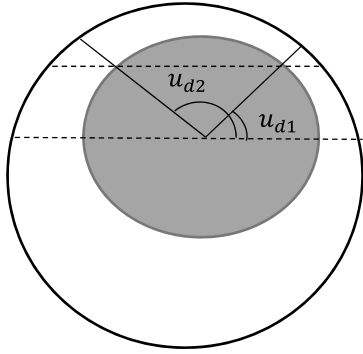
Fig. 3   Argument of latitude at target latitude.

calculate a value of θ that satisfies Eq. (6). From this, the corresponding $u_d = (\theta + \omega)$ values can be readily calculated. There are always two values of u for which the spacecraft is over the target latitude, as illustrated in Fig. 3.

These two values are related by the equation

$$\mathrm{mod}(u_{d1} + u_{d2}, 2\pi) = \pi \tag{7}$$

Regardless of which u value the bisection method returns, the other can be calculated using Eq. (7).

For each calculated value of u, a value of $u + 2\pi k$, in which k is an integer, will also provide proper latitude targeting. As will be shown in Sec. IV, the latitude controllability of the system can be assessed to determine the minimum and maximum values of k. For all possible u_d values, the increase in true anomaly ($\Delta\theta_d$) required for latitude targeting can be calculated based on the initial u_i as

$$\Delta\theta_d = \mathrm{mod}(u_d - u_i, 2\pi) \tag{8}$$

Section IV.A shows that the $\Delta\theta_d$ that results from an increase in t_{swap} is given by

$$\Delta\theta_d = \omega_{a2} \Delta t_{\mathrm{swap}} \left(1 - \frac{C_{b1}}{C_{b2}}\right) \tag{9}$$

The increase in t_{swap} necessary to produce a desired $\Delta\theta_d$ is thus

$$\Delta t_{\mathrm{swap}} = \frac{\Delta\theta_d C_{b2}}{\omega_{a2}(C_{b2} - C_{b1})} \tag{10}$$

in which ω_{a2} is the average angular velocity during phase 2 of the orbit shown in Fig. 4. The deorbit locations associated with all t_{swap} values that provide latitude targeting are recorded along with the corresponding longitude errors. The t_{swap} value that yields the lowest correctable longitude error should be chosen.
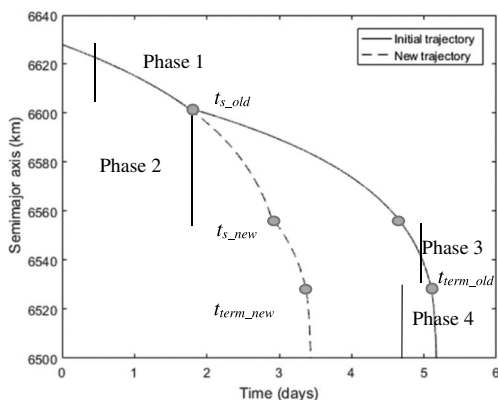

Fig. 4   Effects of only changing swap time.

For a given longitude error $\lambda_e = \lambda_{\mathrm{act}} - \lambda_{\mathrm{des}}$, the increase in orbit lifetime necessary to correct for this error is

$$\Delta t_d = \frac{\lambda_e}{\omega_e} \tag{11}$$

in which ω_e is the rotation rate of Earth. The fact that the mean motion of the spacecraft at larger semimajor axes is less than at lower semimajor axes makes it possible to change the total orbit lifetime without varying the total change in true anomaly by manipulating the amount of time the satellite spends at each altitude. This facilitates a change in the deorbit longitude without a change in latitude.

Using the variables ($t_{s_{\mathrm{old}}}$, $t_{s_{\mathrm{new}}}$, C_{b10}, C_{b20}, C_{b1}, C_{b2}, $\Delta\theta_{10}$, $\Delta\theta_{20}$, $\Delta\theta_1$, $\Delta\theta_2$, $\Delta\theta_t$, Δt_{10}, Δt_{20}, Δt_1, Δt_2, Δt_t), Eqs. (2) and (3), and knowledge of an initial numerically propagated trajectory, we can calculate the control parameters necessary for a new trajectory to achieve a desired Δt_t (time to terminal point). Note that, for the variables listed earlier, a subscript 1 indicates a parameter value between the initial time and t_{swap}, whereas a subscript 2 denotes a value between t_{swap} and t_{term}. Variables with the subscript zero correspond to the initial trajectory, and those without the zero correspond to the new trajectory. The subscripts old and new are also used to differentiate between the trajectories. The subscript t (for total) indicates a value between the initial time and t_{term}. No changes are made to the spacecraft's C_{b_term}, and the drag configurations are swapped at the same semimajor axis in the new and initial trajectories. Given the relations

$$\Delta\theta_1 + \Delta\theta_2 = \Delta\theta_t \tag{12}$$

$$\Delta t_1 + \Delta t_2 = \Delta t_t \tag{13}$$

$$\Delta\theta_1 = \frac{\Delta\theta_{10} C_{b10}}{C_{b1}} \tag{14}$$

$$\Delta\theta_2 = \frac{\Delta\theta_{20} C_{b20}}{C_{b2}} \tag{15}$$

$$\Delta t_1 = \frac{\Delta t_{10} C_{b10}}{C_{b1}} \tag{16}$$

$$\Delta t_2 = \frac{\Delta t_{20} C_{b20}}{C_{b2}} \tag{17}$$

the C_{b1} and C_{b2} required to achieve the desired $\Delta\theta_t$ and Δt_t can be solved for analytically as

$$C_{b2} = \frac{C_{b20}(\Delta t_{20}\Delta\theta_{10} - \Delta t_{10}\Delta\theta_{20})}{(\Delta t_t)(\Delta\theta_{10}) - (\Delta t_{10})(\Delta\theta_t)} \tag{18}$$

$$C_{b1} = \frac{\Delta\theta_{10} C_{b10} C_{b2}}{\Delta\theta_t C_{b2} - \Delta\theta_{20} C_{b20}} \tag{19}$$

In this case, $\Delta\theta_t$ will be the same as in the trajectory with t_{swap} calculated for latitude targeting, and Δt_t will be the original orbit lifetime plus the desired increase in orbit lifetime necessary for longitude targeting (Δt_d) given by Eq. (11). Note that only the drag profile before the terminal point will be manipulated by the targeting algorithm, and so the time to deorbit and the total change in true anomaly and right ascension of the new trajectory after the terminal point will be the same as for the initial trajectory after this point. Because Eqs. (12–19) assume that the swap points occur at the same semimajor axes for the new and initial trajectories, it will be necessary to update $t_{s_{\mathrm{new}}}$ so that this is the case. This is performed by imposing

$$t_{s_{\text{new}}} = \frac{t_{s_{\text{old}}} C_{b10}}{C_{b1}} \qquad (20)$$

This procedure analytically finds a set of control parameters that will result in minimized latitude- and longitude-targeting errors based on the last available numerically propagated trajectory. This analytical solution facilitates the numerical-optimization process diagrammed in Fig. 1.

IV. Controllability Analysis

A. Latitude Controllability

If the maneuver initiates with insufficient orbit life remaining; if poor initial C_{b1}, C_{b2}, and t_{swap} values are chosen; or if the ballistic coefficient of the spacecraft cannot be varied significantly, the spacecraft may be unable to target the desired longitude and latitude. This section investigates the factors that contribute to the controllability of the system [13].

First, let us consider the effects on the impact location of deviations in the value of only t_{swap} from an initial trajectory. Consider the case, in which t_{swap} is increased, whereas C_{b1} and C_{b2} remain constant. Changing t_{swap} will mean that phase 2 of the new trajectory (the phase between $t_{s_{\text{old}}}$ and $t_{s_{\text{new}}}$) will have a different time and change in true anomaly than phase 2 of the initial trajectory (assuming that C_{b1} and C_{b2} are not identical). The total changes in true anomaly and times required for phases 1, 3, and 4 of the new trajectory will be the same as in the initial trajectory, as illustrated in Fig. 4. If t_{20} is the time required for phase 2 of the initial trajectory, the time t_2 required for phase 2 in the new trajectory is equal to the change in t_{swap} and is related to t_{20} by Eq. (2) as

$$\Delta t_{\text{swap}} = t_2 = \frac{C_{b2} t_{20}}{C_{b1}} \qquad (21)$$

The total increase in orbit lifetime resulting from the increase in t_{swap} is then given by

$$\Delta t_d = t_2 - t_{20} = \Delta t_{\text{swap}} \left(1 - \frac{C_{b1}}{C_{b2}}\right) \qquad (22)$$

Once the change in orbit lifetime has been calculated, the difference in the total change in true anomaly between the new and old trajectories can be calculated by

$$\Delta \theta_d = \omega_{a2} \Delta t_d \qquad (23)$$

in which ω_{a2} is the average angular velocity during phase 2 and is calculated based on the initial trajectory.

If t_{swap} in the new trajectory is set to its maximum possible value, phase 3 in Fig. 4 will not exist and the maximum t_{swap} can be written as

$$t_{s_{\text{max}}} = t_{s_{\text{old}}} + (t_{\text{term}_{\text{old}}} - t_{s_{\text{old}}}) \frac{C_{b2}}{C_{b1}} \qquad (24)$$

From the set of possible swap times, the one that results in minimum latitude error and the minimum correctable longitude error should be chosen. The ability to change orbit lifetime by at least 12 h guarantees that the target longitude will pass beneath the orbital plane at least once and that the longitude error will be no greater than Earth's angle of rotation over half an orbital period. The worst-case longitude error from a variation of only t_{swap} is thus about 1250 km for an equatorial target location, but is usually much less. In Fig. 5, the solid lines represent deorbit points that can be reached through a variation of only t_{swap}. In the left image, the area between the solid and dashed lines represents the additional points that can be targeted through longitude control if the maximum spacecraft C_b is 0.025 m^2/kg and the minimum is 0.01 m^2/kg. Because the right image represents a much higher initial altitude, the set of feasible points that can be targeted through longitude control spans the entire Earth at all latitudes below the orbital inclination and is not plotted.

B. Longitude Controllability

Once the most desirable t_{swap} value has been determined, C_{b1} and C_{b2} must be varied to eliminate the remaining longitude error by changing the orbit lifetime without varying the total change in true anomaly. The maximum amount by which the orbit lifetime can be varied in this manner will depend on the characteristics of the initial trajectory and the selected t_{swap} value. If ω_{10} is the average orbital angular velocity between the initial time and $t_{\text{swap}} (\Delta t_{10})$ in the initial trajectory and ω_{20} is the average angular velocity between t_{swap} and $t_{\text{term}} (\Delta t_{20})$, we can rewrite Eq. (18) as

$$C_{b2} = \frac{C_{b20}[\Delta t_{20}(\omega_{10} - \omega_{20})]}{(\Delta t_{20})(\omega_{10} - \omega_{20}) + (\Delta t_d)\omega_{10} - (\Delta \theta_d)} \qquad (25)$$

Assuming $\Delta \theta_d = 0$ (no desired difference in change in true anomaly between the trajectories) and solving for Δt_d yield

$$\Delta t_d = \frac{\Delta t_{20}(\omega_{10} - \omega_{20})}{\omega_{10}} \left(\frac{C_{b20}}{C_{b2}} - 1\right) \qquad (26)$$

For a given value of C_{b2}, the C_{b1} needed to ensure $\Delta \theta_d = 0$ is calculated using Eq. (19), and the resulting increase in orbit lifetime
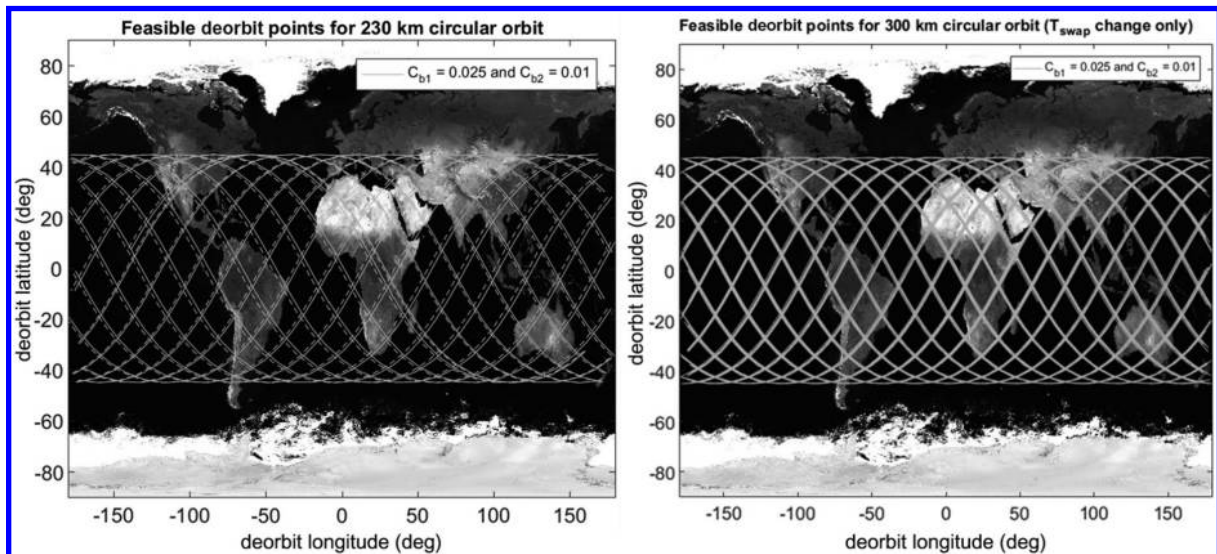

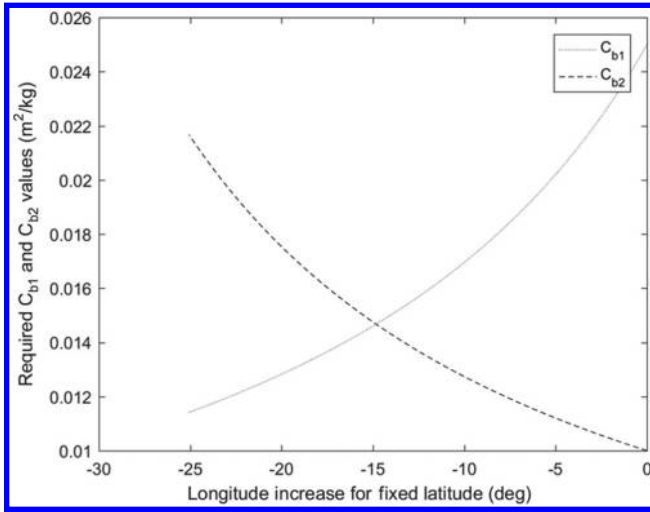**Fig. 5 Feasible deorbit locations with aerodynamic control.**

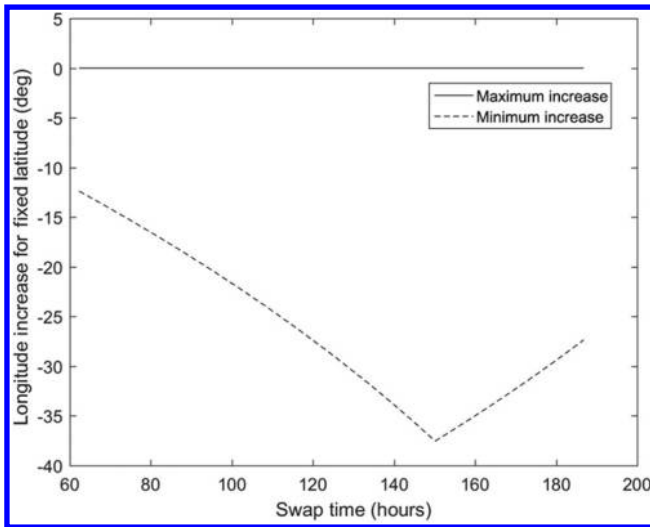Fig. 6   Cb values required to produce given changes in longitude.

Fig. 7   Maximum and minimum longitude increase.

(Δt_d) is given by Eq. (26). Figure 6 illustrates the C_b values required to achieve various increases in the deorbit longitude (given by $-\Delta t_d \omega_e$) for a 300 km initial circular orbit with a t_{swap} value of 480,000 s (133.3 h), $C_{b10} = 0.025$ m^2/kg, and $C_{b20} = 0.01$ m^2/kg. Note that, for certain Δt_d values, the required C_{b1} and C_{b2} values may not be physically attainable.

The maximum and minimum Δt_d values (for $\Delta \theta_d = 0$) are determined by the minimum and maximum C_{b1} and C_{b2} values. To find the maximum Δt_d value, choose the maximum possible C_{b2} value that does not require C_{b1} to be below the minimum value for Eq. (19) to be satisfied with $\Delta \theta_t = \Delta \theta_{10} + \Delta \theta_{20}$. This extends the orbit life for a given total change in true anomaly because the satellite remains at a large semimajor axis for as long as possible and experiences a slower mean motion. Similarly, the minimum Δt_d (usually negative) occurs at the minimum possible C_{b2} value that does not require C_{b1} to be above the maximum value for Eq. (19) to be satisfied with $\Delta \theta_t = \Delta \theta_{10} + \Delta \theta_{20}$. Before performing longitude targeting, the minimum and maximum values of Δt_d corresponding to feasible combinations of C_{b1} and C_{b2} should be computed. It is important to note that the closer a t_{swap} value is to the beginning or end of the orbit lifetime, the more limited the longitude controllability will be, as shown in Fig. 7 for a 300 km initial circular orbit with $C_{b10} = C_{b\,max} = 0.025$ m^2/kg, and $C_{b20} = C_{b\,min} = 0.01$ m^2/kg. For this set of initial conditions, there is sufficient controllability to target any desired deorbit location with a latitude below the orbit inclination.

V.   Software Implementation and Simulation Results

A.   Targeting-Algorithm Process

The targeting algorithm uses the previously discussed principles and procedures to generate a ballistic-coefficient profile (C_{b1}, C_{b2}, t_{swap}) that a spacecraft must follow to deorbit in a desired location. The numerically propagated trajectory associated with this ballistic-coefficient profile is called the guidance, and the spacecraft will continually modulate its ballistic coefficient to track this guidance. Algorithms for spacecraft rendezvous using differential drag [10,14] could be used for guidance tracking, but they are not the focus of this Note and will not be discussed further. Additionally, measurement of the aerodynamic drag force from onboard accelerometers can be used to help characterize the uncertainties in the drag force and modulate the ballistic coefficient to minimize drift from the guidance. This implementation of the guidance generator closely follows the diagram in Fig. 1 with a minor modification. The latitude-targeting algorithm is conducted first using a variation of only t_{swap}. Once a numerically propagated trajectory is created with minimal latitude error, the longitude-targeting sequence is activated. This process continues until a trajectory is created with zero latitude error, and the minimum possible longitude error or a maximum number of iterations is reached.

In this implementation, the terminal point was set to a mean semimajor axis of 6528 km, and the spacecraft was considered to have reentered the atmosphere when its distance from the center of Earth was 6448 km (approximately 70 km altitude). For propagations beyond the first one, the terminal point was specified by a time value (t_{term}) instead of a mean semimajor-axis value, because even the mean semimajor axis oscillates slightly. This was done by estimating the times required during phases 1, 2, and 3 of each new trajectory (see Fig. 2) and summing the times together to get the new t_{term}.

This method provided targeting convergence even for highly perturbed, eccentric orbits (tested up to $e = 0.01$) because the effects of the perturbations and noncircular orbits were captured in the numerically propagated trajectories.

B.   Orbit Propagator and Initial Guidance Conditions

An orbit propagator was created in MATLAB considering gravitational perturbations through degree and order four, atmosphere rotating with Earth, and NRLMSISE-00 density using historical F10.7 and A_p values. This propagator was validated against the high-precision orbit propagator (HPOP) contained in the Systems Tool Kit (STK)simulation suite and agreed within less than 3% error after over a week of propagation. The guidance generator was also configured to optionally use the HPOP propagator directly, and the optimizer converged in all scenarios where this was done, proving the robustness of the solution process with high-fidelity propagators. In practice, the choice of when to start guidance generation depends on the mission at hand and the capabilities of the satellite. If a spacecraft must be landed in a very precise area and significant computational power is available, guidance generation should start two or more weeks before deorbit to ensure sufficient longitude controllability to target the desired deorbit point. The authors considered the more

Table 1   MC simulation parameters

| Variable	Range	Distribution
Semimajor axis	[6668, 6778] km	Uniform
True anomaly	[0, 360] deg	Uniform
Eccentricity	[0, 0.004]	Uniform
Right ascension	[0, 360] deg	Uniform
Argument of the periapsis	[0, 360] deg	Uniform
Inclination	[1, 97] deg	Uniform
Impact latitude	[0, inclination −0.1] deg	Uniform
Impact longitude	[−180, 180] deg	Uniform
$C_{b\,max}$	[0.033, 0.067] m^2/kg	Uniform
$C_{b\,min}$	[0.0053, 0.027] m^2/kg	Uniform
Epoch	[1 November 2003, 1 November 2014]	Uniform
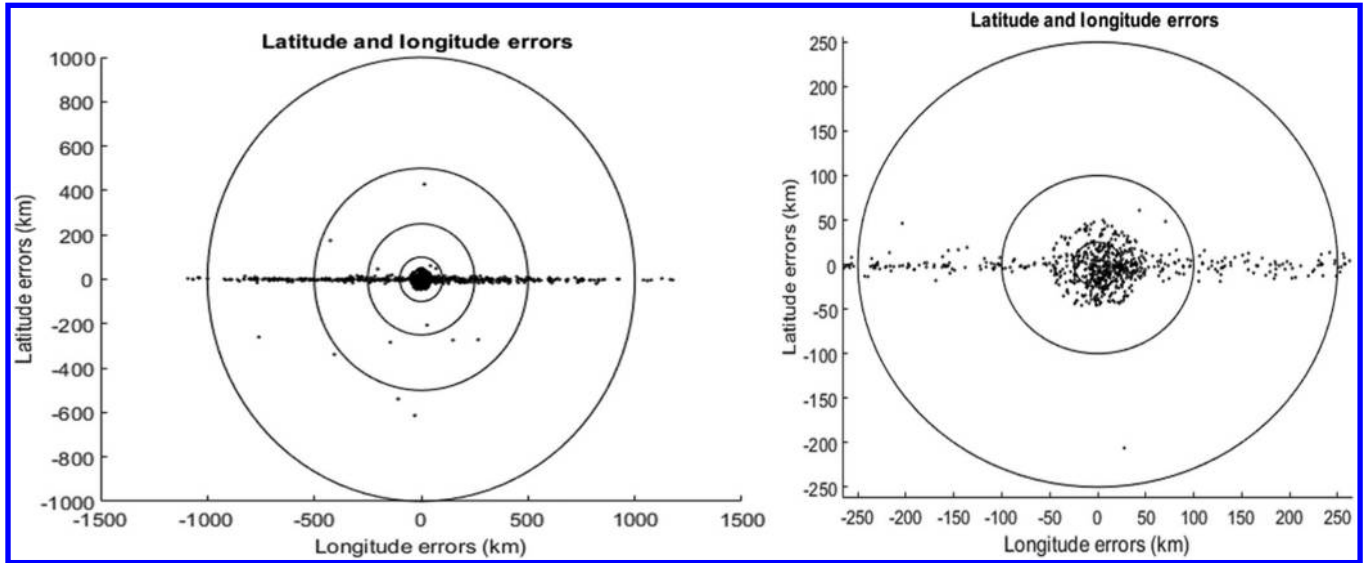
Fig. 8 Latitude and longitude errors (right graph zoomed in).

Table 2 Average simulation results

Simulation parameter	Average value
Total error, km	199.4
Longitude error, km	192.5
Latitude error, km	13.94
Orbit lifetime, day	5.5
Simulation run time, min	20.7

common case to be one in which a spacecraft with limited computing power and limited drag control must deorbit somewhere over a wide oceanic region to prevent debris from falling over populated areas. In this case, a longitude error of up to ±1250 km is acceptable, and guidance generation can begin at a lower altitude. This enables the rapid creation of realistic and trackable guidances.

C. Monte Carlo Simulations

To analyze the effectiveness of the targeting algorithm, a set of 1000 Monte Carlo (MC) simulations with various initial conditions and target locations was conducted. Parameters were randomly selected from uniform distributions within the ranges given in Table 1.

The semimajor-axis range corresponds to average altitudes between approximately 290 and 400 km. This is a common range for the deployment of low-Earth-orbit (LEO) satellites, and targeting would be unlikely to begin at any higher altitude. Note that, although orbits at the upper altitude range may last for several months, guidance generation was set to begin when the satellite had 1 week of orbit lifetime remaining in the minimum drag configuration. The upper bound on eccentricity was set to 0.004 because the mean eccentricity of the International Space Station has not exceeded 0.004 based on data between the years 2000 and 2016 from the STK spacecraft database [15]. Satellites in LEOs tend to naturally circularize due to higher drag at the perigee while the space station experiences greater eccentricities due to the frequent thrusting maneuvers required to maintain altitude. The minimum and maximum ballistic-coefficient ranges correspond to what may be reasonable for small, LEO satellites with maneuverable drag devices. The epoch range spans 11 years because average density experiences a long-term cyclic variation with a period of 11 years corresponding to the solar cycle. Runs were conducted on a desktop PC with a 3.6 GHz Intel i7 processor using MATLAB R2016a. After 1000 MC simulation runs, all cases had an error below 1250 km, which was the predicted upper error bound for cases of limited longitude controllability. Figure 8 shows the distribution of latitude and longitude errors for all the runs.
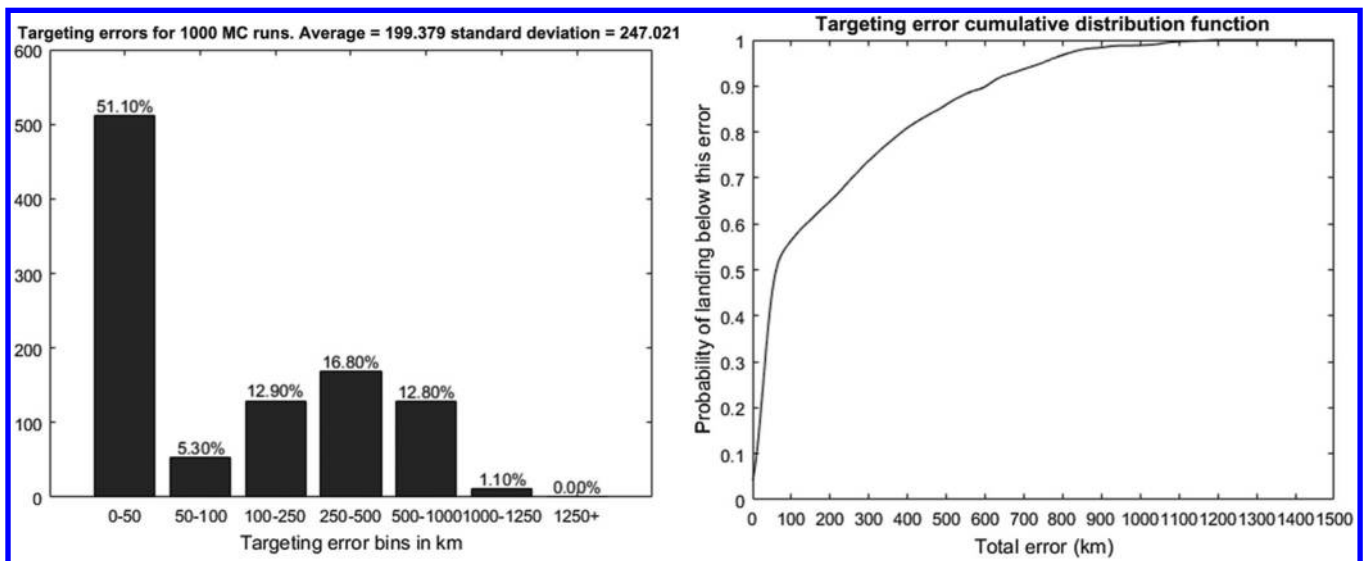

Fig. 9 Targeting-error histogram and CDF.

Table 2 displays relevant average MC results. Figure 9 displays a histogram of the targeting errors and the error cumulative distribution function (CDF).

When the targeting algorithm is run closer to the end of the orbit life, although there will be less discrepancy between the analytical and numerical solutions and the algorithm will converge more quickly, the controllability will suffer, especially the longitude controllability. Table 2 shows that longitude error tends to be significantly greater than latitude error due to this more limited longitude controllability.

According to sec. 4.7.2.1 of the NASA debris mitigation guidelines [16], a selected trajectory for guided reentry must ensure that no surviving debris impact with a kinetic energy greater than 15 J is closer than 370 km from foreign landmasses, or is within 50 km from the continental United States, territories of the United States, and the permanent ice pack of Antarctica. Furthermore, the product of the probability of failure to track the guidance and the risk of human casualty associated with the failure must be less than 0.0001 (1:10,000). In reality, a spacecraft would likely break apart and become a debris cloud upon reaching the reentry point. Mission designers must investigate the expected profile of the debris cloud and pick a target deorbit point, such that all debris fall sufficiently far from land. The existence of longitudinal guidance errors of up to ± 1250 km can be accepted as reasonable because a probable target point for debris mitigation would be somewhere in the South Pacific Ocean Uninhabited Area. For cases in which higher precision is needed, guidance generation must begin sooner to achieve greater controllability.

VI. Conclusions

Through mathematical analysis and simulations, the feasibility of targeting a deorbit location with a spacecraft using solely aerodynamic drag has been demonstrated. Although drag only acts in the orbital plane and hence cannot create an inclination change, any point on Earth below the satellite's inclination can be targeted using aerodynamic drag if maneuvering begins early enough. A numerical-optimization scheme (targeting algorithm) based on an analytical solution was developed to calculate the ballistic-coefficient profile necessary for a LEO spacecraft to deorbit in the desired location. A high-fidelity simulation environment was created for use in the targeting algorithm taking into account a nonspherical Earth, atmospheric rotation, and NRLMSISE-00 density. The algorithm was tested in this environment with 1000 MC runs conducted using a set of randomized initial conditions. The algorithm converged for all cases with a total targeting error under 1250 km. Most of this error was longitudinal. Such an error level is sufficient to meet the NASA debris mitigation guidelines for spacecraft disposal.

Although the average algorithm run time in MATLAB was nearly 21 min, significant performance improvements will be gained by rewriting the code in C++, facilitating guidance computation onboard a spacecraft.

In practical applications, the numerically propagated trajectory with the ballistic-coefficient profile necessary to deorbit in the desired location would serve as the spacecraft guidance. The spacecraft's ballistic coefficient would then be continuously modulated using attitude changes, or the deploying and retracting of a drag device to ensure that the spacecraft follows that guidance.

References

[1] Patera, R. P., and Ailor, W. H., "The Realities of Reentry Disposal," *Proceedings of the AAS/AIAA Space Flight Mechanics Meeting*, American Astronomical Soc., Monterey, CA, 1998, pp. 9–11.

[2] Ailor, W. H., and Patera, R. P., "Spacecraft Re-Entry Strategies: Meeting Debris Mitigation and Ground Safety Requirements," *Journal of Aerospace Engineering*, Vol. 221, No. 6, June 2007, pp. 947–953. doi:10.1243/09544100JAERO199

[3] Moe, K., and Moe, M. M., "Gas–Surface Interactions and Satellite Drag Coefficients," *Planetary and Space Science*, Vol. 53, No. 8, July 2005, pp. 793–801. doi:10.1016/j.pss.2005.03.005

[4] Pérez, D., and Bevilacqua, R., "Neural Network Based Calibration of Atmospheric Density Models," *Acta Astronautica*, Vol. 110, May 2015, pp. 58–76. doi:10.1016/j.actaastro.2014.12.018

[5] Omar, S. R., and Wersinger, J. M., "Satellite Formation Control Using Differential Drag," *Proceedings of the 53rd AIAA Aerospace Sciences Meeting*, AIAA Paper 2015-0002, 2015.

[6] Pérez, D., and Bevilacqua, R., "Differential Drag-Based Reference Trajectories for Spacecraft Relative Maneuvering Using Density Forecast," *Journal of Spacecraft and Rockets*, Vol. 53, No. 1, Jan. 2016, pp. 234–239. doi:10.2514/1.A33332

[7] Pastorelli, M., Bevilacqua, R., and Pastorelli, S., "Differential-Drag-Based Roto-Translational Control for Propellant-Less Spacecraft," *Acta Astronautica*, Vol. 114, Sept. 2015, pp. 6–21. doi:10.1016/j.actaastro.2015.04.014

[8] Dutta, S., Bowes, A., Dwyer Cianciolo, A. M., Glass, C., and Powell, R. W., "Guidance Scheme for Modulation of Drag Devices to Enable Return from Low Earth Orbit," *AIAA Atmospheric Flight Mechanics Conference*, Paper 0467, Jan. 2017.

[9] Virgili, J., and Roberts, P., "Atmospheric Interface Reentry Point Targeting Using Aerodynamic Drag Control," *Journal of Guidance, Control, and Dynamics*, Vol. 38, No. 3, 2015, pp. 403–413. doi:10.2514/1.G000884

[10] Mazal, L., Pérez, D., Bevilacqua, R., and Curti, F., "Spacecraft Rendezvous by Differential Drag Under Uncertainties," *Journal of Guidance, Control, and Dynamics*, Vol. 39, No. 8, Aug. 2016, pp. 1721–1733. doi:10.2514/1.G001785

[11] Vallado, D., *Fundamentals of Astrodynamics and Applications*, 4th ed., Microcosm Press, Hawthorne, CA, 2013, p. 636.

[12] Curtis, H., *Orbital Mechanics for Engineering Students*, 2nd ed., Elsevier, Burlington, MA, 2009, p. 79, 231.

[13] Franklin, G., Powell, J., and Emami-Naeini, A., *Feedback Control of Dynamic Systems*, 4th ed., Prentice–Hall, Upper Saddle River, NJ, 2002, pp. 849–855.

[14] Pérez, D., and Bevilacqua, R., "Differential Drag Spacecraft Rendezvous Using an Adaptive Lyapunov Control Strategy," *Acta Astronautica*, Vol. 83, Feb.–March 2013, pp. 196–207. doi:10.1016/j.actaastro.2012.09.005

[15] Analytical Graphics Inc., *Systems Tool Kit*, Exton, PA.

[16] Anon., "Process for Limiting Orbital Debris," NASA STD-8719.14A, May 2012.

This article has been cited by:

1. Sanny R. Omar, Riccardo Bevilacqua. 2019. Hardware and GNC solutions for controlled spacecraft re-entry using aerodynamic drag. *Acta Astronautica* **159**, 49-64. [Crossref]

2. S.F. Rafano Carná, R. Bevilacqua. 2019. High fidelity model for the atmospheric re-entry of CubeSats equipped with the Drag De-Orbit Device. *Acta Astronautica* **156**, 134-156. [Crossref]

3. S.F. Rafano Carná, S. Omar, D. Guglielmo, R. Bevilacqua. 2019. Safety analysis for shallow controlled re-entries through reduced order modeling and inputs' statistics method. *Acta Astronautica* **155**, 426-447. [Crossref]

4. David Guglielmo, Sanny Omar, Riccardo Bevilacqua, Laurence Fineberg, Justin Treptow, Bradley Poffenberger, Yusef Johnson. 2019. Drag Deorbit Device: A New Standard Reentry Actuator for CubeSats. *Journal of Spacecraft and Rockets* **56**:1, 129-145. [Abstract] [Full Text] [PDF] [PDF Plus]